Performance Investigation and Power Factor Improvement of a Consequent-Pole Type Bearingless Motor

Junichi Asama*
Shizuoka University
Hamamatsu, Japan

Masatsugu Takemoto
Hokkaido University
Sapporo, Japan

Hiroya Sugimoto
Tokyo Institute of Technology
Tokyo, Japan

Akira Chiba
Tokyo Institute of Technology
Tokyo, Japan

Abstract

The authors have developed a five-axis actively positioned bearingless drive system intended for a use as an industrial contamination-free centrifugal pump. It includes 1.2 kW consequent-pole type bearingless motor for torque generation and radial/tilting motion control. The aim of this paper is to investigate the motor performance with a test machine. In addition, a proposed rotor is found to improve power factor of a motor function. Based on the three-dimensional finite element method (3D-FEM) analysis, the effectiveness of the proposed structure has been verified in this paper.

1 Introduction

To realize practical use in special environment of the electrical motor, a bearingless motor, which combines function of both motor and magnetic bearing [1] in a single unit, has been developed [2]. A bearingless motor possesses the advantages of not only non-mechanical-contact operation, but also a simple structure, a compactness, and a cost reduction in comparison to the conventional magnetic bearings. Bearingless motors are practically applied to contamination-free centrifugal pumps in industries where contamination of pumping fluid should be avoided, such as chemical pumps [3, 4], ventricular assist devices [5-7], and bioreactors [8].

Bearingless contamination-free chemical pumps with a mechanical output of 50 W, 300 W, and 900W are practically used in semiconductor and liquid crystal industries or an industry where special clean environment is required. This pioneering bearingless motor is originated from Levitronix GmbH and ETH Zurich, Switzerland [3]. In this bearingless pump, a surface-mounted permanent magnet (SPM) type of bearingless motor with two-axis radial active positioning is employed. These bearingless motors are notable in small pump applications. In the applications more than a few kW, five-axis active positioning is used because the rotor has rather long axial length with respect to the slice structure. The authors have previously proposed a five-axis actively positioned bearingless motor system, intended for a use as a contamination-free centrifugal pump [9]. A magnetic air-gap is designed to be wider than that in conventional bearingless motors. Because of five-axis active magnetic suspension control, undesirable axial and conical movements caused by dynamic fluid force are not occurred during pumping.

In [9], suspension characteristics of the fabricated test machine have been demonstrated. To avoid complicated assembly process, a thrust magnetic bearing with a cylindrical rotor is installed into the test machine as an alternative to a conventional thrust magnetic bearing with a disk rotor [10]. In this paper, motor performance of the test machine has been investigated. In addition, a novel rotor structure of the bearingless motor for further power factor improvement has been proposed. Based on the three-dimensional finite element method (3D-FEM) analysis, the effectiveness of the proposed structure has been verified in this paper.

*Contact Author Information: tjasama@ipc.shizuoka.ac.jp, 3-5-1 Johoku, Naka-ku, Hamamatsu, Japan, 432-8561, Tel: +81-53-478-1033, Fax: +81-53-478-1041

2 Motor Performance

Figure 1 shows a schematic of a developed five-axis actively positioned bearingless motor and a fabricated test machine. Radial and tilting motions of the rotor are actively regulated by the bearingless motor units. The thrust position of the rotor is actively controlled by the thrust magnetic bearing. The proposed bearingless motor is an extension of a hybrid of consequent-pole and homo-polar bearingless motors. Two bearingless motor units are connected in tandem. A thrust magnetic bearing is installed at the end of one bearingless motor unit, although it is not shown in Figure 1. One rotor unit consists of the consequent-pole rotor and a cylindrical iron core. Radially magnetized permanent magnets are inset between the rotor iron cores. Magnetized direction of the radial permanent magnets in one unit is opposite to that in the other one. In the left unit in Figure 1, magnetic poles on the surface of the permanent magnets are S-pole. The bias flux, produced by a permanent magnet ring between the stators, flows through the stators, air-gaps, rotor cores, and a shaft, so that the iron cores are consequently magnetized. Therefore, iron cores in the left unit in Figure 1 are magnetized as N-pole. The proposed bearingless motor, thus, works as an eight-pole synchronous machine. The stator has two kinds of windings: eight-pole motor winding and two-pole suspension winding, which are concentratedly wound around the teeth. The principle of suspension force generation is similar to that of a homo-polar magnetic bearing. The suspension force is generated by flux unbalance in the air-gap, which is caused by superimposing two-pole suspension flux to the bias magnetic flux.

All permanent magnets used in the bearingless motor are NdFeB. Rotor cores used in the stator and the rotor are laminated steel, and the shaft is made of bulk iron. An outer diameter and an axial length of the test machine are 186 mm and 182 mm, respectively. An arc angle of the radial permanent magnet is 40°. Three copper wires for motor windings are wound in parallel. The number of turns in one tooth is 39. A self-inductance in one phase is 1.1 mH, and d-axis and q-axis inductances are 2.8 mH and 3.0 mH, respectively. A flux linkage is 24.6 mWb. The rated mechanical output, torque, and rotational speed are 1.2 kW, 2 Nm, and 6000 r/min, respectively.

Figure 2(a) shows measured induced voltage in each phase at 5000 r/min. In the waveforms, 2nd harmonic component is included. Figure 2(b) shows root-mean-square values of fundamental, 2nd and 4th harmonic components. Fundamental component increases by 5.7 V as the rotational speed increases by 1000 r/min. The 2nd harmonic component is caused by magnetic flux distribution of the consequent-pole rotor [11].

Figure 3 shows measured motor performances of the test machine. The targeted mechanical output of 1.2 kW is achieved at 6000 r/min with a torque current of 15.3 A. When the motor output is 1256 W, efficiency, power factor, active input power, apparent power, copper loss, and sum of mechanical and iron losses are 64.6 %, 0.35, 1940 W, 3230 VA, 634 W, and 54 W, respectively. Figure 3 (d) shows measured phase currents when the maximum power of 1256 W is produced. Ratios of 2nd and 4th harmonics to fundamental component in the waveforms are 11 % and 2 %, respectively. Although the targeted output can be achieved, power factor is considerably low with respect to conventional permanent magnet motors.

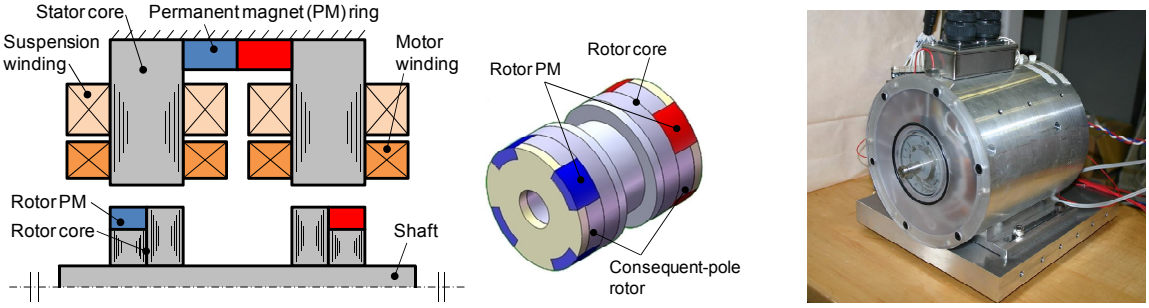

(a) Schematic (thrust magnetic bearing is not shown) (b) Fabricated test machine

Figure 1: Developed five-axis actively positioned consequent-pole type bearingless motor

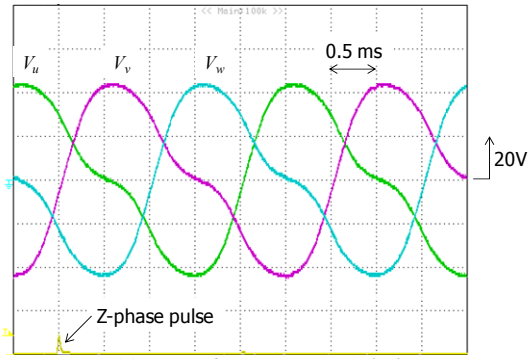

(a) Waveforms at 5000 r/min

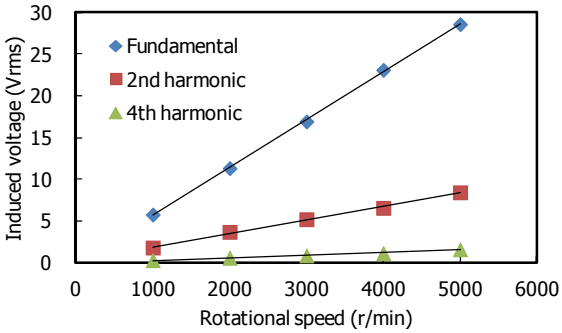

(b) RMS value against rotational speed

Figure 2: Measured induce voltage.

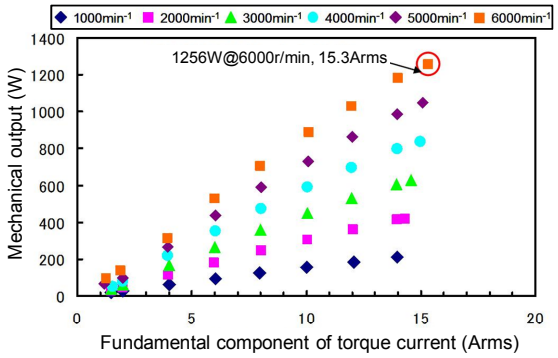

(a) Mechanical output

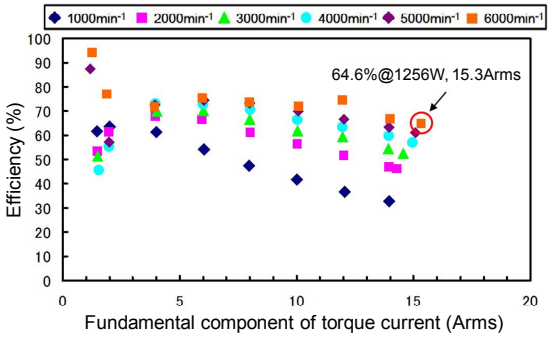

(b) Efficiency

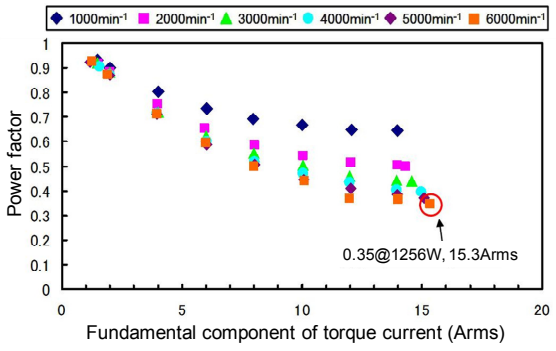

(c) Power factor

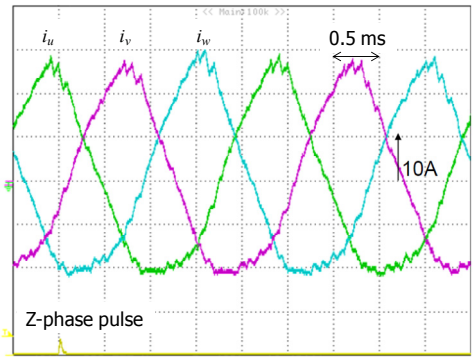

(d) Phase current at 6000 r/min with 2 Nm

Figure 3: Measured motor performances of the test machine

3 Power Factor Improvement

In order to improve the power factor of the test machine, an effective solution is proposed in this section by using commercially available FEM software (JMAG, JSOL Corp., Japan). The power factor $\cos\phi$ is calculated as:

$$\cos\phi = \frac{1}{\sqrt{1+\left(\frac{L}{\psi} I_q\right)}} \tag{1}$$

where L is self-inductance, I_q is torque current, and Ψ is flux linkage. Thus, reduction of inductance is effective for an improvement of power factor. Figure 4 shows the proposed rotor structure [12]. The proposed rotor is an extension of a hybrid of SPM and homo-polar rotors. The consequent-pole rotors in Figure 1 are replaced with SPM rotors. Figure 5 shows calculated power factor against radial thickness of the permanent magnet t_r. When t_r=9 mm, the calculated power factor is approximately 0.73. Figure 6 shows calculated power factor against axial length of the laminated rotor core h. As h is decreased, the power factor is improved because of reduction in self-inductance.

Figure 7 shows calculated radial suspension force in X- and Y-axis with X-axis suspension current. The force variation, which is defined as the ratio of the maximum difference from the average to the average, is 34 % in X-axis with the proposed SPM rotor, although it is 8% with the conventional consequent-pole rotor. Maximum value of undesirable force component in Y-axis with X-axis suspension current is 20 N, which is about 20 % of the average of X-axis suspension force. Figure 8 shows error angle of the suspension force, defined as $\tan^{-1}(F_y/F_x)$. The maximum error angle is 14°. Although the power factor is significantly improved, variation and error angle of the suspension force becomes large. The force variation and error angle should be as small as possible for stable magnetic suspension control. These considerable variations of the proposed rotor are reduced by the improved rotor structure presented in the later section.

Figure 9 shows counter plot of bias magnetic flux density of the SPM rotor when the motor and suspension currents are 0 A. Magnetic saturation is seen in the rotor core part around S-pole rotor magnet, which may cause the

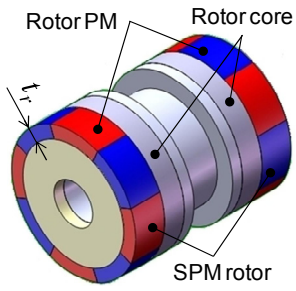

Figure 4: Proposed SPM rotor structure for power factor improvement

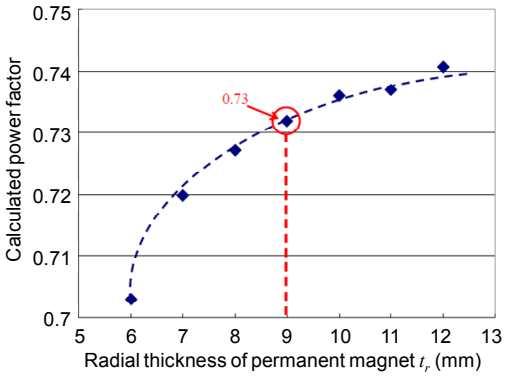

Figure 5: Calculated power factor against radial thickness of permanent magnet t_r

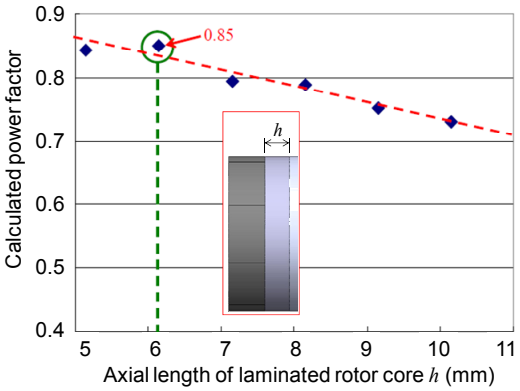

Figure 6: Calculated power factor against axial length of laminated rotor core h

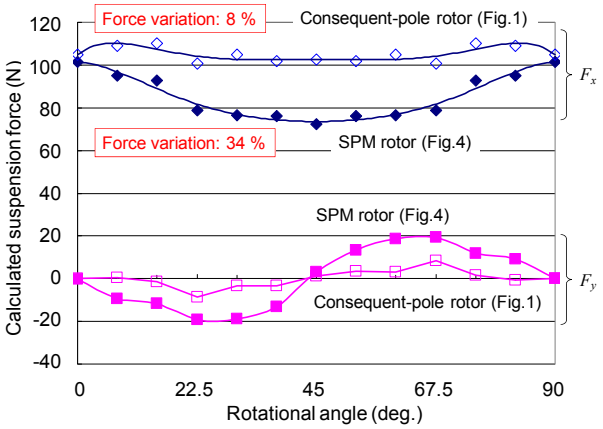

Figure 7: Calculated suspension force in X- and Y-axis with X-axis suspension current (h=6mm)

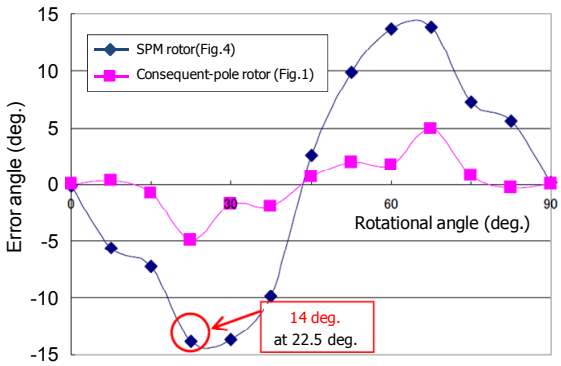

Figure 8: Calculated error angle of suspension force with X-axis suspension current (h=6mm)

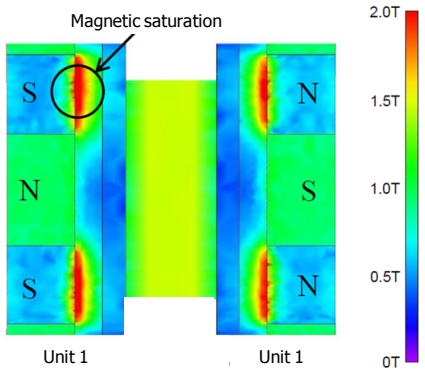

Figure 9: Contour plot of magnetic flux density

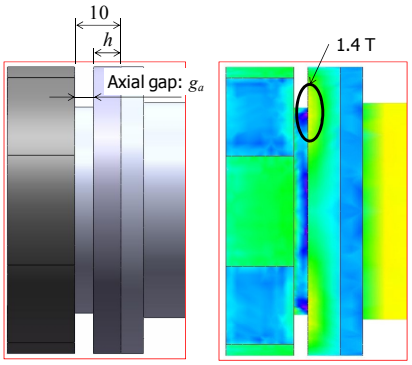

Figure 10: Improved rotor structure with axial gap g_a

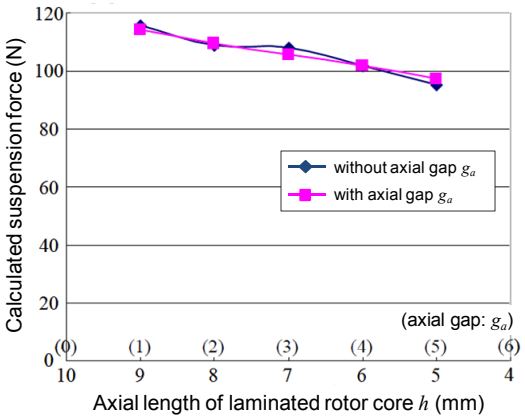

Figure 11: Calculated suspension force with or without axial gap g_a

significant force variation and error angle. This magnetic saturation is caused by bias magnetic flux induced from both the radial S-pole rotor magnet and the stator permanent magnet. To reduce the magnetic saturation, a further improved rotor structure is proposed as shown in Figure 10. An axial air-gap g_a is provided between the rotor magnet and the rotor core. As a result, the saturation can be reduced to 1.4 T, as shown in Figure 10.

Figure 11 shows calculated suspension force with or without axial gap g_a. When g_a is provided, the sum of axial length of the rotor core h and axial gap g_a is determined to 10 mm. When g_a is increased, the suspension force is decreased because an axial length of the rotor core is decreased. However, the suspension force of approximately 100 N is achieved. Figure 12 shows calculated force variation with or without axial gap g_a. When g_a is provided, the average of the force variation is decreased by 13 %. In addition, the error angle is also decreased by 7.4° as shown in Figure 13. The axial gap g_a has been verified to be effective for reduction of variation and error angle of the suspension force. Figure 14 shows calculated power factor with axial gap g_a. When g_a=3 mm and h=7mm, the calculated power factor is 0.8.

The force variation remains 18 %, which is relatively large for bearingless motor. It can be solved by employing sub-coil arrangement in the suspension windings, as shown in Figure 15 [13]. To reduce the suspension force variation, an improved suspension winding configuration employing sub-coils is applied. Additional short pitch coils are wound around the stator teeth located at both sides of the main coil. The MMF direction of the sub-coil is the same as that of the main coil. The sub-coils contribute to decreasing the harmonic components of the MMF distribution. Figure 16 shows calculated radial suspension force with the sub-coil arrangement. The force variation is significantly reduced from 18 % to 1 %. In addition, the error angle is reduced from 3° to 1°. Table 1 shows performance comparison of a conventional consequent-pole rotor (Figure 1) and a improved SPM rotor (Figure 4)

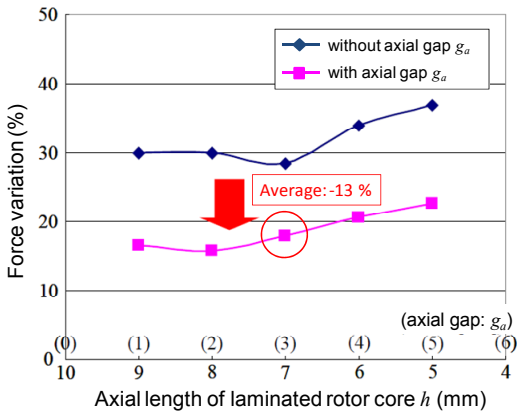

Figure 12: Calculated force variation with or without axial gap g_a

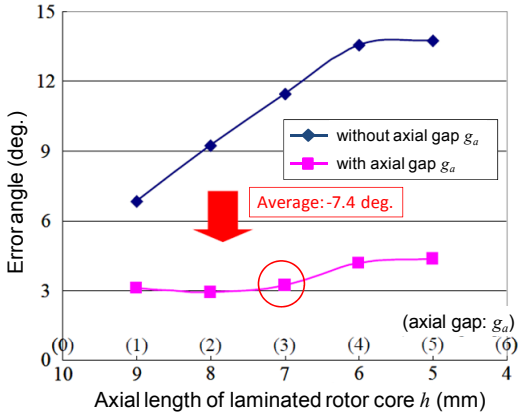

Figure 13: Calculated error angle with or without axial gap g_a

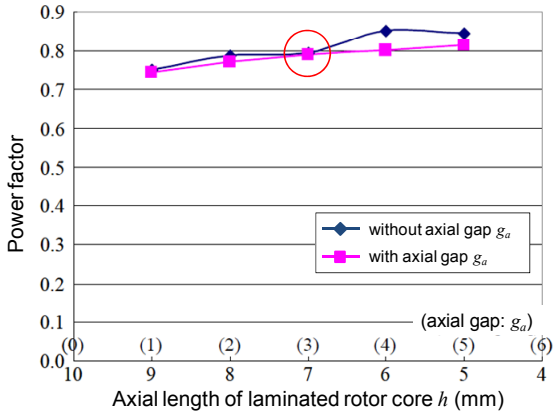

Figure 14: Calculated power factor with or without axial gap g_a

with sub-coil arrangement. The power factor of a motor function is significantly improved from 0.35 to 0.8. Variation and error angle of the suspension force are reduced to 1 % and 1°, respectively.

4 Conclusions

The motor performance of the proposed five-axis actively positioned bearingless motor has been investigated. The proposed bearingless motor is an extension of a hybrid of consequent-pole and homo-polar bearingless motors. Although the targeted mechanical output of 1.2 kW can be achieved, the measured power factor of the test machine is 0.35 which is low with respect to conventional permanent magnet motors. To improve the power factor, the hybrid rotor structure of SPM and homo-polar rotors is proposed. Based on the FEM analysis, the motor performances with the proposed SPM rotor have been calculated. An improved rotor structure is also proposed to reduce force variation. The calculated results have demonstrated that the power factor is increased more than 0.8.

Acknowledgement

The authors would like to acknowledge the contribution to this research project of Mr. Naoya Miyamoto and Mr. Takehiro Enomoto, who were with the Chiba Laboratory as former graduate students in the Department of Electrical Engineering, Faculty of Science and Technology, Tokyo University of Science, Japan.

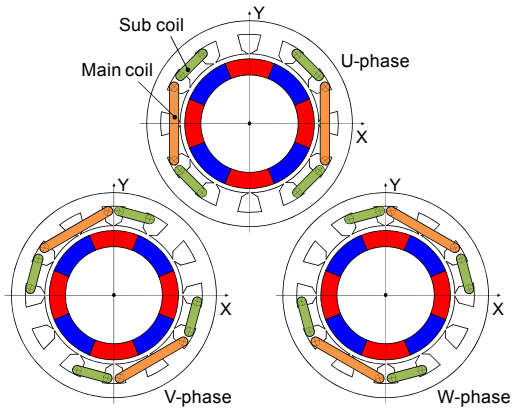

Figure 15: Improved suspension winding arrangement with sub-coils

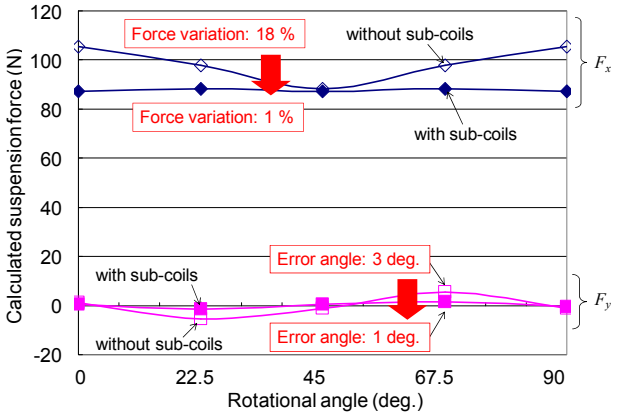

Figure 16: Calculated suspension force with sub-coil arrangement

	Conventional consequent-pole rotor	Improved SPM rotor
Power factor	0.35	0.8
Force variation	8 %	1 %
Error angle	5°	1°

Table 1: Performance comparison of a conventional consequent-pole rotor and a improved SPM rotor

References

[1] G. Schweitzer, E. H. Maslen, *et., al.*. Magnetic Bearings, Springer, 2009, ISBN: 978-3642007964.

[2] A. Chiba, T. Fukao, *et., al.*. Magnetic Bearings and Bearingless Drives, Newnes, 2005, ISBN: 978-0750657273

[3] R. Schöb and N. Barletta. Principle and Application of a Bearingless Slice Motor, JSME (The Japan Society of Mechanical Engineers) International Journal, Series C, Vol. 40, No. 4, pp. 593-598, 1997.

[4] M. Neff, N. Barleetta, and R. Schöb. Bearingless Centrifugal Pump for Highly Pure Chemicals, in Proceedings of the 8th International Symposium on Magnetic Bearings, pp. 283-288, Mito, Japan, August 26-28, 2002.

[5] R. Schöb, N. Barletta, *et., al.*. A Bearingless Motor for a Left Ventricular Assist Device (LVAD), in Proceedings of the 7th International Symposium on Magnetic Bearings, Zurich, Switzerland, August 23-25, 2000.

[6] T. Masuzawa, T. Kita, K. Matsuda, and Y. Okada. Magnetically Suspended Rotary Blood Pump with Radial Combined Mtor-Bearing. Artificial Organs, Vol. 26, No. 4, pp. 468-474, 2000.

[7] J. Asama, A. Chiba, T. Oiwa, T. Fukao, and M. A. Rahman. A Design Consideration of a Novel Bearingless Disk Motor for Artificial Hearts, in Proceedings of the IEEE Energy Conversion Congress and Exposition (ECCE) 2009, pp. 1693-1699, Sep. 19-24, San Jose, California, USA, 2009.

[8] T. Reichert, T. Nussbaumer, and J. W. Kolar. Bearingless 300 W PMSM for Bioreactor Mixing. IEEE Transactions on Industrial Electronics, Vol. 59, No. 3, pp. 1376 - 1388, March 2012.

[9] J. Asama, M. Amada, *et., al.*. Evaluation of a Bearingless PM Motor with Wide Magnetic Gaps, IEEE Transactions on Energy Conversion, Vol. 25, No. 4, pp. 957-964, December 2010.

[10] J. Asama, N. Miyamoto, T. Enomoto, M. Amada, A. Chiba, and T. Fukao. A Novel Design of a Thrust Magnetic Bearing with a Cylindrical-Shaped Rotor, in Proceedings of IEEE Power Engineering Society General Meeting 2009, Jul. 26-30, Calgary, Albert, Canada, 2009.
[11] J. Asama, M. Amada, A. Chiba, M. Takemoto, T. Fukao, and M. A. Rahman. Voltage Characteristics of a Consequent-pole Bearingless PM Motor with Concentrated Windings. IEEE Transactions on Magnetics, Vol. 45, Issue 6, pp. 2823-2826, June 2009.
[12] N. Yamamoto, M. Takemoto, S. Ogasawara, and M. Hiragushi. Experimental Estimation of a 5-AXIS Active Control Type Bearingless Canned Motor Pump, in Proceedings of IEEE International Electric Machines and Drives Conference 2011, pp. 148-153, May 15-18, Niagara Falls, Canada, 2011.
[13] J. Asama, R. Kawata, T. Tamura, T. Oiwa, and A. Chiba. Reduction of Force Interference and Performance Improvement of a Consequent-Pole Bearingless Motor. Precision Engineering, Vol. 36, Issue 1, pp. 10-18, January 2012.